Nanoscale

PAPER

View Article Online
View Journal | View Issue

Cite this: *Nanoscale*, 2014, **6**, 4698

Phase transformation and enhanced photocatalytic activity of S-doped Ag_2O/TiO_2 heterostructured nanobelts†

W. J. Zhou,*[a] Y. H. Leng,[b] D. M. Hou,[c] H. D. Li,[b] L. G. Li,[a] G. Q. Li,[c] H. Liu*[b] and S. W. Chen[ad]

Received 11th December 2013
Accepted 23rd January 2014

DOI: 10.1039/c3nr06565k

www.rsc.org/nanoscale

Ag_2O/TiO_2 nanobelt heterostructures have been found to possess high ultraviolet photocatalytic activity, but a poor cycling performance. After a S-doping treatment, the obtained $Ag_2O/Ag_2S_2O_7/TiO_2$ heterostructured nanobelts exhibited an enhanced and stable photocatalytic activity under both ultraviolet and visible light irradiation, which was exemplified by photo-degradation of organic pollutants and photocurrent response measurements. Meanwhile, the crystal structure and phase transformation of Ag_2O, $Ag_2S_2O_7$ and Ag_2S were studied by XRD and XPS measurements.

Introduction

Titanium dioxide (TiO_2), as an efficient photocatalyst, has been intensively investigated since Fujishima and Honda discovered the photocatalytic splitting of water on TiO_2 electrodes in 1972.[1] TiO_2 has been shown to be an excellent photocatalyst due to its long-term stability, low-cost preparation and a strong oxidizing power useful for the decomposition of unwanted organic compounds.[2–5] However, this material is only active under UV excitation because of its large energy band gap of 3.2 eV (in its anatase form). Considering that the fraction of UV light is less than 5% in the total solar spectrum on the earth, it is crucial and a great challenge to develop efficient, visible light-active photocatalysts. Thus, band gap engineering of photocatalysts to induce absorption into the wide visible light region has been considered as a possible solution to this problem. The doping of anions such as N,[6,7] H,[8,9] and C[10] into TiO_2 has been widely reported. In addition, the growth of TiO_2-based heterostructures, such as Ag_2O/TiO_2,[11] Cu_xO/TiO_2,[12] MoS_2/TiO_2[13] and Fe_2O_3/TiO_2,[14] and $SrTiO_3/TiO_2$[15] have been developed, aiming to enhance the photocatalytic efficiency by broadening their light-harvesting window into the visible range. At the same time, the efficiency of charge separation can be enhanced by coupling two semiconductor structures with matching energy levels, leading to improved photocatalytic activity.[16–19]

Previously, we developed a new system of Ag_2O/TiO_2 nanobelts, which can effectively suppress the hole–electron recombination under UV light irradiation.[11] Ag_2O nanoparticles have been found to act as efficient electron absorbing agents under UV light irradiation and as an efficient photosensitiser under visible light irradiation.[11,20,21] Subsequently, many studies on the synthesis of Ag_2O photocatalysts have been reported, such as Ag_2O,[20,22] Ag_2O/ZnO,[23] Ag_2O/Bi_2O_3,[24] Ag_2O/TiO_2,[25] Ag_2O/Ag_2CO_3,[26] graphene oxide/Ag_2O[27] and g-C_3N_4/Ag_2O.[28] In our work, we found that the Ag_2O/TiO_2 heterostructures possess a high photocatalytic activity, but a poor cycling performance, as Ag_2O may be reduced into Ag by photogenerated electrons.[11] Thus, in order to improve the stability of these photocatalysts, surface plasmon effects and core–shell structures have been used to prevent photocorrosion, as shown in the preparation of Ag/AgCl[29] and $Cu_2O@TiO_2$[30] hybrid structures. Herein, we designed a new approach based on the S-doping of Ag_2O onto TiO_2 nanobelts to prepare $Ag_2O/Ag_2S_2O_7/TiO_2$ heterostructures that exhibit high and stable photocatalytic activity, under both ultraviolet and visible light irradiation. $Ag_2S_2O_7$ on the surface of Ag_2O can effectively protect Ag_2O from conversion to Ag. The crystal structure and phase transformation of Ag_2O, $Ag_2S_2O_7$ and Ag_2S were studied by X-ray diffraction (XRD) and X-ray photoelectron spectroscopy (XPS).

Experimental

Chemicals

Titania P25 (a commercial TiO_2), sodium hydroxide (NaOH), hydrochloric acid (HCl), sulfuric acid (H_2SO_4), silver nitrate ($AgNO_3$), and sodium sulfide (Na_2S) were purchased from

[a]*New Energy Research Institute, School of Environment and Energy, South China University of Technology, Guangzhou Higher Education Mega Center, Guangzhou 510006, China. E-mail: eszhouwj@scut.edu.cn*

[b]*State Key Laboratory of Crystal Materials, Center of Bio & Micro/Nano Functional Materials, Shandong University, 27 Shandanan Road, Jinan 250100, China. E-mail: hongliu@sdu.edu.cn*

[c]*School of Materials Science and Engineering, South China University of Technology, Wushan Road, Tianhe, Guangzhou 510006, China*

[d]*Department of Chemistry and Biochemistry, University of California, 1156 High Street, Santa Cruz, California 95064, USA*

† Electronic supplementary information (ESI) available: Additional characterization and experimental details. See DOI: 10.1039/c3nr06565k

Sigma-Aldrich Co. LLC. All chemicals were used without further purification. Deionized water was used throughout all experiments.

Synthesis of TiO_2 nanobelts with a rough surface

The TiO_2 nanobelts with a rough surface were synthesized through a simple hydrothermal procedure, followed by an acid corrosion treatment.[4] In a typical reaction, 0.1 g of TiO_2 powder (P25) was mixed with 20 mL of 10 M NaOH aqueous solution. The mixed solution was stirred and then transferred into a Teflon-lined stainless steel autoclave, heated at 180 °C for 48 h, and then air-cooled to room temperature. The obtained wet powder was washed thoroughly with deionized water followed by a filtration process. The obtained $Na_2Ti_3O_7$ nanobelts were immersed in 0.1 M HCl aqueous solution for 24 h and then washed thoroughly with distilled water to obtain the H-titanate ($H_2Ti_3O_7$) nanobelts. To roughen the surface, the obtained $H_2Ti_3O_7$ nanobelts were added into a 25 mL Teflon vessel, then filled with 20 mL of 0.02 M H_2SO_4 aqueous solution and maintained at 100 °C for 12 h. Finally, the products were isolated from the solution by centrifugation and sequentially washed with deionized water several times, and dried at 70 °C for 10 h. By annealing the acid-corroded $H_2Ti_3O_7$ nanobelts at 600 °C for 2 h, anatase TiO_2 nanobelts with a rough surface were obtained.

Synthesis of Ag_2O/TiO_2 nanobelt heterostructures

The formation process of the Ag_2O/TiO_2 nanobelt heterostructures (50 wt% of Ag_2O) was as follows.[11] Typically, 0.2 g of the acid-corroded TiO_2 nanobelts prepared above was dispersed in 50 mL of distilled water and 0.29 g of silver nitrate ($AgNO_3$) was then dissolved into the suspension. The mixture was stirred magnetically for 30 min to establish the adsorption equilibrium. 50 mL of a 0.2 M NaOH aqueous solution was slowly dropped into the above mixture of $AgNO_3$ and TiO_2. The amount of NaOH was more than sufficient to completely consume all the added $AgNO_3$, and the final pH of the reaction solution was 14. Finally, the TiO_2 nanobelts coated by Ag_2O nanoparticles were collected after centrifugation and washed with deionized water several times, then dried at 50 °C for 12 h.

Synthesis of S-doped Ag_2O/TiO_2 nanobelts heterostructures

0.2 g of the Ag_2O/TiO_2 nanobelt heterostructures (50 wt% of Ag_2O) prepared above was dispersed in 50 mL of distilled water, then stirred magnetically for 30 min. A calculated amount of an aqueous solution of 0.01 M sodium sulfide (Na_2S) was slowly added into the above suspension during the magnetic stirring. The color of the suspension was found to gradually change from yellow to black. S-doped Ag_2O/TiO_2 nanobelts were produced and collected after centrifugation and sequentially washed with deionized water several times, then dried at 50 °C for 12 h. The different components of the heterostructures were controlled by adding different amounts of sulfur; 0 mg, 8.4 mg, 16.8 mg and 33.6 mg of Na_2S were added into the above aqueous solution of 0.2 g Ag_2O/TiO_2. The obtained heterostructures were denoted as S1 (Ag_2O/TiO_2), S2 ($Ag_2O/Ag_2S_2O_7/TiO_2$), S3 ($Ag_2S_2O_7/TiO_2$) and S4 (Ag_2S/TiO_2), respectively.

Characterizations

The X-ray powder diffraction (XRD) patterns of the catalysts were recorded with a Bruke D8 Advance powder X-ray diffractometer with Cu Kα ($\lambda = 0.15406$ nm). A HITACHI S-4800 field emission scanning electron microscope (FE-SEM) was used to characterize the morphologies and size of the synthesized Ag_2O/TiO_2 samples. The chemical composition was investigated *via* energy-dispersive X-ray spectroscopy (EDS). The high resolution transmission electron microscopic (HRTEM) images were acquired with a JOEL JEM 2100 microscope. UV-vis absorption spectra were recorded with a UV-vis spectrophotometer (UV-2600, Shimadzu) with an integrating sphere attachment and $BaSO_4$ as a reflectance standard. X-ray photoelectron spectroscopy (XPS) was performed using an ESCALAB 250 instrument.

Photocatalytic degradation activity under UV and visible light irradiation

Methyl orange (MO, 20 mg L^{-1}) was selected as the model chemical to evaluate the activity and properties of the different photocatalysts. In a typical experiment, 20 mL of an aqueous solution of MO and 20 mg of photocatalyst powders were placed into a 50 mL beaker. Prior to photoirradiation, the suspensions were magnetically stirred in the dark for 30 min to establish an adsorption–desorption equilibrium between the dye and the catalysts under ambient conditions. A 350 W mercury lamp with a maximum emission of 356 nm was used as the UV resource, and a 300 W Xe arc lamp through a UV-cutoff filter ($\leq$420 nm) was used as the visible light source. At different irradiation intervals, an aliquot of the reaction solution was collected, centrifuged to remove the catalyst, and used to measure the concentration of MO by monitoring the absorbance with a UV-vis spectrophotometer (UV-2102PC). The different samples were repeatedly used six times with the same experimental conditions to test the photocatalytic stability.

Photocurrent measurements

For the fabrication of the photoelectrodes, 1 mL of an ethanol suspension of the as-prepared photocatalyst powders (20 mg) was dropcast onto a piece of indium tin oxide (ITO) glass with a cover area of 1 cm^2 and allowed to dry under ambient conditions. The photocurrents were measured with an electrochemical workstation (CHI 750E, CH Instruments Inc., Shanghai) using a three-electrode mode in an aqueous solution of 1 M Na_2SO_4. The reference electrode and counter electrode were a Ag/AgCl electrode (saturated KCl) and platinum wire, respectively. The as-prepared photoelectrodes were used as the anodes for the electrochemical characterizations. A 350 W mercury lamp with a maximum emission at 356 nm was used as the UV resource with a light intensity of 450 mW cm^{-2}. A 300 W Xe arc lamp through a UV-cutoff filter ($\leq$420 nm) was used as the visible light source with a light intensity of 220 mW cm^{-2}.

Results and discussion

The XRD patterns of Ag_2O/TiO_2, $Ag_2O/Ag_2S_2O_7/TiO_2$, $Ag_2S_2O_7/TiO_2$ and Ag_2S/TiO_2 nanobelt heterostructures are shown in Fig. 1, which illustrate the phase transformation of Ag_2O by S-doping. In curves (a) to (c), one can see a series of diffraction peaks at 25.2, 37.7, 47.9, 53.8, 55 and 62.5° which are assigned to the anatase TiO_2 (JCPDS files no. 21-1272); and the diffraction peaks at 32.8, 38 54.9 and 65.4° in the pattern of Ag_2O/TiO_2 correspond to the cubic structure of Ag_2O (JCPDS files no. 41-1104). After a full vulcanization treatment, pure Ag_2S was obtained, with the corresponding diffraction peaks at 29, 31.5, 33.6, 34.4, 34.7, 36.5, 36.8, 37.1, 37.7, 40.7 and 43.4° (JCPDS files no. 14-0072), as depicted in Fig. 1d. In comparison with the diffraction profiles of Ag_2O/TiO_2 and Ag_2S/TiO_2, the peaks of the partially S-doped Ag_2O nanoparticles at 20.5, 32.6 and 33.6° are attributed to $Ag_2S_2O_7$ (JCPDS files no. 21-1343, Fig. 1b and c). The Ag_2O, $Ag_2S_2O_7$ and TiO_2 phases coexist in the S2 sample (Fig. 1b), which indicates that $Ag_2S_2O_7$ is the metastable interphase between Ag_2O and Ag_2S.

The morphological and microstructural details of the as-prepared Ag_2O/TiO_2, $Ag_2O/Ag_2S_2O_7/TiO_2$, $Ag_2S_2O_7/TiO_2$ and Ag_2S/TiO_2 nanobelt heterostructures were then investigated by SEM and HRTEM measurements. Fig. 2a shows a typical SEM image of the as-prepared Ag_2O/TiO_2 nanobelts. The acid corroded nanobelts show a width of 50 to 200 nm, and a length of up to hundreds of microns, which is shown in Fig. S1.† The Ag_2O nanoparticles on the TiO_2 nanobelts exhibited a narrow size distribution with a small size of 5 to 20 nm. However, the Ag_2O nanoparticles can't be distinguished from the TiO_2 nanobelts with a rough surface by SEM equipment due to the low contrast.[4,11] The energy dispersive X-ray spectroscopy (EDS) analysis (Fig. 2e) reveals that the Ag_2O/TiO_2 nanobelts are only composed of Ag, Ti and O elements. After the sulfur doping, the morphologies of the nanobelt heterostructures of $Ag_2O/Ag_2S_2O_7/TiO_2$, $Ag_2S_2O_7/TiO_2$ and Ag_2S/TiO_2 remained virtually unchanged as shown in Fig. 2b–d, indicating the nanoparticles on TiO_2 nanobelts are very stable. The EDS analysis reveals that the sulfur content of the heterostructures increased with the doping contents, which is shown in Fig. 2e.

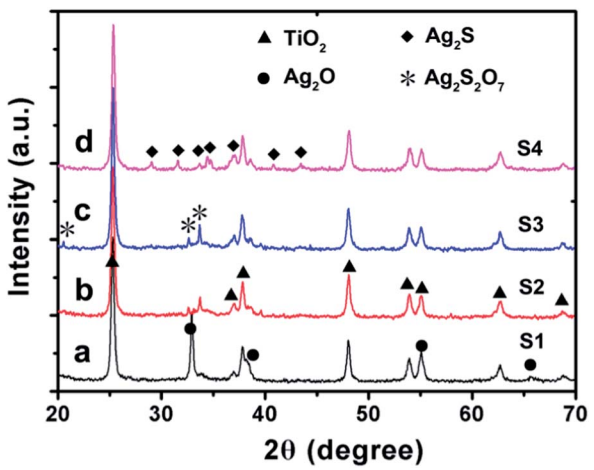

Fig. 1 The XRD patterns of (a) Ag_2O/TiO_2, (b) $Ag_2O/Ag_2S_2O_7/TiO_2$, (c) $Ag_2S_2O_7/TiO_2$ and (d) Ag_2S/TiO_2 nanobelt heterostructures.

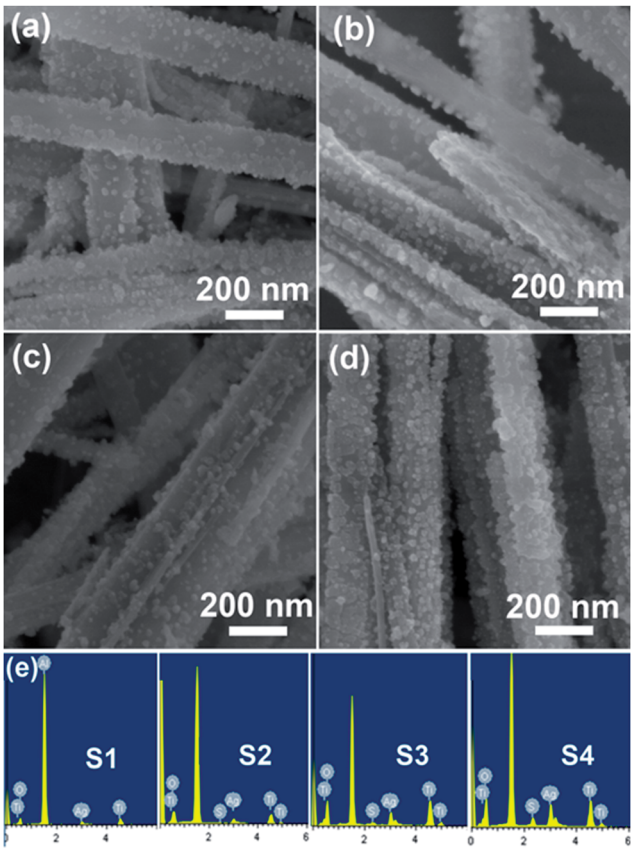

Fig. 2 Typical SEM images of (a) Ag_2O/TiO_2, (b) $Ag_2O/Ag_2S_2O_7/TiO_2$, (c) $Ag_2S_2O_7/TiO_2$ and (d) Ag_2S/TiO_2 nanobelt heterostructures with different magnifications and (e) the EDS results of the different heterostructures.

The HRTEM images of the samples further confirm the formation of a heterostructure between the TiO_2 nanobelt and $Ag_2S_2O_7$ nanoparticles (Fig. 3). After a Na_2S aqueous solution was added into the mixed aqueous solution of Ag_2O/TiO_2 nanobelts, $Ag_2S_2O_7$ nanoparticles were found to be tightly attached to the surface of the TiO_2 nanobelt, forming $Ag_2S_2O_7/TiO_2$ heterostructures (Fig. S2†), which may be propitious to electron transfer between the two phases. Measurements of the lattice fringes showed an interplanar distance of *ca.* 0.35 nm and 0.14 nm, corresponding to the (101) plane of anatase TiO_2 and the (220) plane of $Ag_2S_2O_7$, respectively. The energy dispersive X-ray spectrometry (EDS) mapping analysis of the S3 sample also confirmed that the $Ag_2S_2O_7$ nanoparticles, composed of Ag, S, and O elements, were dispersed on the surface of the TiO_2 nanobelt with Ti and O signals (Fig. 3c). In addition, the obscure interfaces on the surface of the Ag_2O nanoparticles were observed in the HRTEM image of S2 ($Ag_2O/Ag_2S_2O_7/TiO_2$) as shown in Fig. S3,† which implies that the $Ag_2S_2O_7$ was possibly formed by sulfur diffusion into the interior Ag_2O nanoparticles.

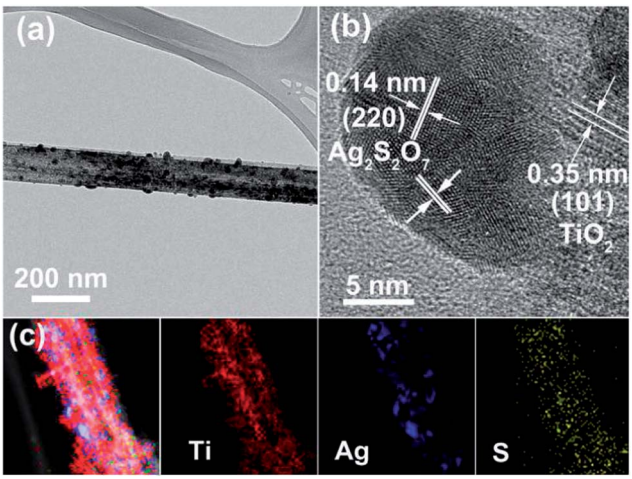

Fig. 3 HRTEM images (a and b) of $Ag_2S_2O_7/TiO_2$ (S3) nanobelt heterostructures with different magnification. (c) EDS mapping results from the $Ag_2S_2O_7/TiO_2$ heterostructure.

The electronic states of the Ag and S elements in the S-doped Ag_2O were then studied by XPS measurements. The results are shown in Fig. 4. The Ag $3d_{5/2}$ electrons of Ag_2O/TiO_2 can be identified at 368.1 eV, which is characteristic of Ag^+ (Fig. 4a). The asymmetric peaks for Ag $3d_{5/2}$ and Ag $3d_{3/2}$ suggest that the Ag_2O nanoparticles might have undergone a partial surface reduction from the photoelectrons of the TiO_2 nanobelts. From sample S2 to sample S4, the binding energy of the Ag $3d_{5/2}$ electrons was found to shift to 367.8, 367.9 and 368 eV, respectively, in good agreement with the expected values for Ag bound to sulfur, indicating the increasing degree of sulfur doping.[31] The XPS measurements of the S 2p electrons display similar results (Fig. 4b). For the Ag_2O/TiO_2 sample, no S signal was observed. After sulfur doping, obvious signals can be observed for the S 2p electrons in the S2, S3 and S4 samples. For instance, for the S2 and S3 samples, in addition to the S^{2-} electrons at 162.9 and 161.7 eV, the S^{6+} electrons can also be at 168.7 and 167.7 eV, indicating the formation of $Ag_2S_2O_7$. After being completely vulcanized (S4), the S^{6+} peaks disappeared, consistent with the complete conversion from $Ag_2S_2O_7$ to Ag_2S. In comparison with the results of Ag_2S, the S 2p peaks for $Ag_2S_2O_7$ shift by about 0.7 eV from 161.0 eV to 161.7 eV, which could be attributed to the S–O bonding effect. These XPS results suggest that the S-doping process might involve a change of the S valence state from S^{2-}(Na_2S) to S^{6+}($Ag_2S_2O_7$), and then to S^{2-}(Ag_2S).

To evaluate the photocatalytic activity, we examined the decomposition of MO in water under UV light irradiation as a function of time. For comparison, the decomposition over (S1) Ag_2O/TiO_2, (S2) $Ag_2O/Ag_2S_2O_7/TiO_2$, (S3) $Ag_2S_2O_7/TiO_2$ and (S4) Ag_2S/TiO_2 was carried out under the same experimental conditions. As shown in Fig. 5a, the Ag_2O/TiO_2 heterostructures exhibited the highest photocatalytic activity of MO degradation under UV irradiation. With increasing irradiation time, the decomposition of the MO dye progressed steadily and completed in 8 min of UV irradiation. The degradation activity of $Ag_2O/Ag_2S_2O_7/TiO_2$ heterostructures was much higher than those of the $Ag_2S_2O_7/TiO_2$, Ag_2S/TiO_2 and TiO_2 nanobelts, and slightly lower than that of Ag_2O/TiO_2. The results suggest that the photocatalytic activity of the heterostructures decreased with the increase of the sulfur content.

Yet, the photocatalytic stability of the heterostructures under UV light irradiation was enhanced with S-doping. Experimentally, the photocatalysts were used repeatedly six times after separation *via* membrane filtration, and the activity was evaluated and compared, as shown in Fig. 5b. One can see that the Ag_2O/TiO_2 photocatalyst was unstable for repeated use under UV irradiation with a marked decrease of photocatalytic activity after each repetition. For instance, the photocatalytic degradation efficiency of MO was only 65% after the sixth time. However, the S-doped samples of $Ag_2O/Ag_2S_2O_7/TiO_2$, $Ag_2S_2O_7/TiO_2$, Ag_2S/TiO_2 photocatalysts all exhibited stable photocatalytic performance under UV light irradiation. There is no obvious decrease of the removal rate of MO after six cycles for 96 min.

The visible-light photocatalytic activities of TiO_2 nanobelts, Ag_2O/TiO_2, $Ag_2O/Ag_2S_2O_7/TiO_2$, $Ag_2S_2O_7/TiO_2$ and Ag_2S/TiO_2 were also evaluated by photocatalytic degradation of a MO aqueous solution under visible light irradiation, which are shown in Fig. 6. Due to the large band gap energy (3.2 eV for anatase), TiO_2 nanobelts can absorb UV light with wavelengths shorter than 400 nm. So, TiO_2 nanobelts showed only a low photocatalytic activity under visible-light irradiation, and the degradation was only 12% in 150 min. In contrast, the Ag_2O/TiO_2, $Ag_2O/Ag_2S_2O_7/TiO_2$, $Ag_2S_2O_7/TiO_2$ and Ag_2S/TiO_2 heterostructured catalysts all showed apparent visible-light photocatalytic activity. Fig. 7 depicts the UV-vis absorbance spectra of

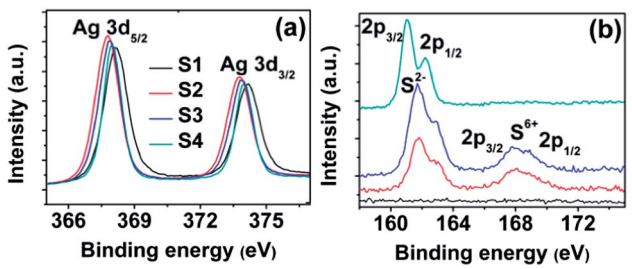

Fig. 4 XPS spectra taken from the samples with different sulfuration extent of Ag_2O on TiO_2 nanobelts: (a) Ag 3d spectra and (b) S 2p spectra.

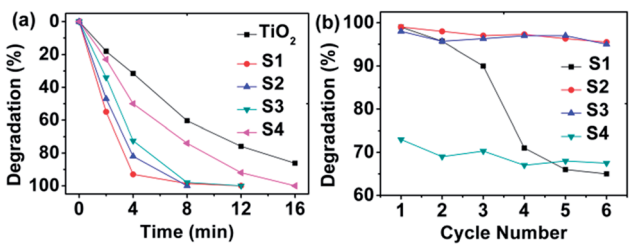

Fig. 5 (a) Photocatalytic activity and (b) stability under UV light irradiation of (S1) Ag_2O/TiO_2, (S2) $Ag_2O/Ag_2S_2O_7/TiO_2$, (S3) $Ag_2S_2O_7/TiO_2$ and (S4) Ag_2S/TiO_2 nanobelt heterostructures and TiO_2 nanobelts.

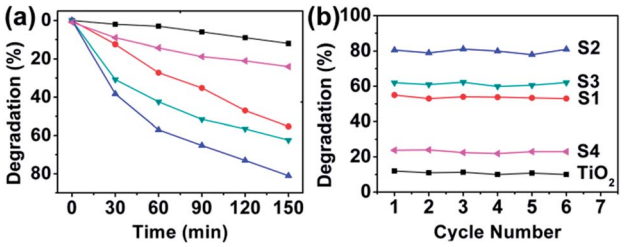

Fig. 6 (a) Visible-light photocatalytic activity and (b) stability of TiO_2 nanobelts, (S1) Ag_2O/TiO_2, (S2) $Ag_2O/Ag_2S_2O_7/TiO_2$, (S3) $Ag_2S_2O_7/TiO_2$ and (S4) Ag_2S/TiO_2.

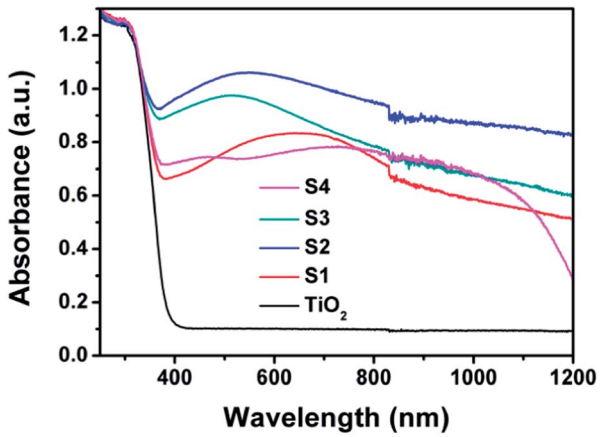

Fig. 7 UV-vis absorbance spectra of TiO_2 nanobelts, (S1) Ag_2O/TiO_2, (S2) $Ag_2O/Ag_2S_2O_7/TiO_2$, (S3) $Ag_2S_2O_7/TiO_2$ and (S4) Ag_2S/TiO_2.

the different samples. One can see that Ag_2O, $Ag_2S_2O_7$ and Ag_2S might act as efficient visible-light sensitizers leading to improved visible light photocatalytic activity of the TiO_2 nanobelts. For instance, Ag_2O/TiO_2 nanobelts display a strong light absorption in both UV and visible regions of 250–1200 nm. After sulfur doping, the obtained $Ag_2O/Ag_2S_2O_7/TiO_2$, $Ag_2S_2O_7/TiO_2$ showed a similar absorption in the same range of 250 nm to 1200 nm but with a blue shift. As for Ag_2S/TiO_2, the absorption peak between 500 and 600 nm disappeared, and the absorbance was significantly reduced at a wavelength greater than 1000 nm. Note that the photocatalytic activity of $Ag_2O/Ag_2S_2O_7/TiO_2$ heterostructure was better than those of Ag_2O/TiO_2, $Ag_2S_2O_7/TiO_2$ and Ag_2S/TiO_2. This might be accounted for by energy band matching that has been found to play an important role in enhancing photocatalytic activity. The degradation rate of MO by $Ag_2O/Ag_2S_2O_7/TiO_2$ reached 81% in 150 min. The corresponding degradation rates of MO under the same conditions in the presence of Ag_2O/TiO_2, $Ag_2S_2O_7/TiO_2$ and Ag_2S/TiO_2 were 55%, 62% and 24%, respectively. To investigate the photocatalytic stability under visible light irradiation, the same samples were repeatedly used for six cycles, which are shown in Fig. 6b. All the heterostructured photocatalysts, (S1) Ag_2O/TiO_2, (S2) $Ag_2O/Ag_2S_2O_7/TiO_2$, (S3) $Ag_2S_2O_7/TiO_2$ and (S4) Ag_2S/TiO_2, exhibited very stable photocatalytic activity under visible-light irradiation. There is no obvious decrease in the degradation rate of MO after six cycles (for 900 min). Of these, the $Ag_2O/Ag_2S_2O_7/TiO_2$ heterostructured nanobelts exhibited the best photocatalytic performance under both UV and visible light irradiation.

To further understand the effects of heterostructures and S-doping on the photocatalytic activity, we studied the photoinduced charge transfer properties of the S-doped Ag_2O/TiO_2 heterostructures. The photocurrent response of the different heterostructures was recorded under UV and visible-light irradiation (λ > 420 nm). Fig. 8a shows the photographs of the different photoelectrodes. The rich colors indicate different energy band structures of the S-doped Ag_2O/TiO_2 heterostructures that might affect photoabsorption. Fig. 8b shows the photocurrent–time curves for S-doped Ag_2O/TiO_2 heterostructures under several on–off light irradiation cycles. All samples generate photocurrents with a reproducible response to on–off cycles under UV light irradiation, demonstrating the effective charge transfer and electron collection for the photoelectrodes. However, only pure TiO_2 nanobelts were fast in generating a photocurrent with a reproducible response to on–off cycles. The S-doped Ag_2O/TiO_2 heterostructures show a longer photo-response time, implying a slower charge transfer process, which is possibly due to the heterostructured interface and the random order of the S-doped Ag_2O/TiO_2 nanobelts. However, sample S1 (Ag_2O/TiO_2) exhibited the highest photocurrent, which is consistent with the UV photocatalytic activity of S-doped Ag_2O/TiO_2 heterostructures (Fig. 5). Under visible-light irradiation, pure TiO_2 nanobelts show only a negligible photocurrent, whereas all S-doped heterostructures show apparent photocurrents, even higher than those under UV light irradiation, such as S2 ($Ag_2O/Ag_2S_2O_7/TiO_2$). The high current

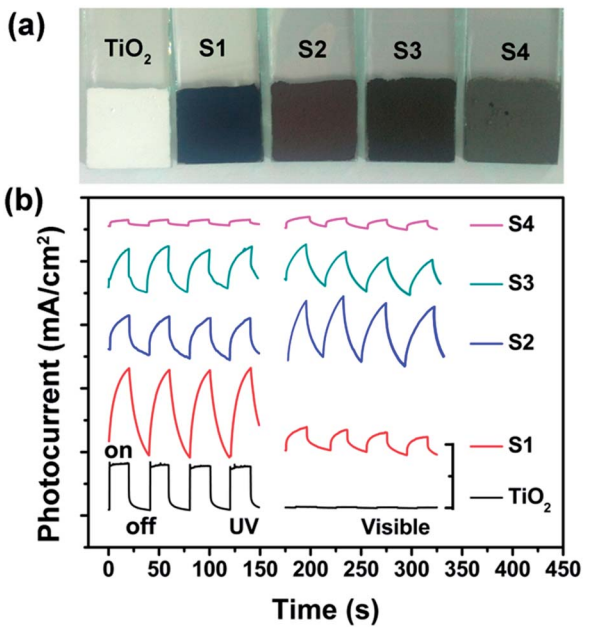

Fig. 8 Photographs (a) and time-dependent photocurrent responses (b) of the ITO photoelectrodes composed of the different heterostructured photocatalysts at a bias voltage of 0.5 V. All of the photocurrent intensities were calibrated with dark current. The scale bar of the y-axis in (b) is 0.5 mA cm^{-2}.

density demonstrates that the photo-induced electrons and holes of $Ag_2O/Ag_2S_2O_7/TiO_2$ prefer to separate and transfer to the ITO glass due to the heterostructures built between Ag_2O, $Ag_2S_2O_7$ and TiO_2.

On the basis of the above results, a possible mechanism of the high and stable photocatalytic activity of the $Ag_2O/Ag_2S_2O_7/TiO_2$ heterostructure under UV and visible light irradiation is proposed (Fig. 9). Standard density functional theory (DFT) was used to calculate the electronic structure of $Ag_2S_2O_7$ herein, which has not been reported up to now. The atomic unit cell structure, band structure and electronic density of states for $Ag_2S_2O_7$ are shown in Fig. S4 and S5.† A band gap of ~2.24 eV for $Ag_2S_2O_7$ was obtained. In addition, the conduction and valence band positions were determined by using the following empirical equation,[32]

$$E_{CB} = X - E_e - 0.5E_g$$

where E_{CB} denotes the conduction band edge potential, X is the geometric mean of the Mulliken electronegativity of the constituent atoms, E_e is the energy of free electrons on the hydrogen scale (about 4.5 eV) and E_g is the band gap. The X values for TiO_2, Ag_2O and $Ag_2S_2O_7$ are 5.81 eV, 5.29 eV and 6.02 eV, respectively,[33] and the corresponding E_g values are 3.2 eV, 1.2 eV, and 2.24 eV. Thus, the positions of the conduction band edge (E_{CB}) at the point of zero charge are estimated to be −0.29 eV, 0.19 eV, and 0.26 eV, respectively, as illustrated in Fig. 9.

Under UV light irradiation, TiO_2 nanobelts were excited to produce holes (h^+) and electrons (e^-). The Ag_2O nanoparticles on the surface of TiO_2 nanobelts captured electrons effectively due to the more positive conduction band of Ag_2O than that of TiO_2. The obtained electrons reacted with the Ag_2O nanoparticles with the narrow band gap (1.2 eV) to produce Ag nanoparticles.[11] The Ag_2O nanoparticles, as electron acceptors, prevent electrons and holes from undergoing recombination, and the holes efficiently oxidize organic compounds, and thus the photocatalytic activity is enhanced, but the catalysts were unstable. After sulfur doping, the obtained $Ag_2S_2O_7$ on the surface of the Ag_2O nanoparticles can effectively prevent deformation of the crystal structure. $Ag_2S_2O_7$ has the appropriate energy structure and energy band matching with that of Ag_2O, to capture electrons from the conduction band of Ag_2O, but not be reduced by the photogenerated electrons of TiO_2 due to the wide band gap of $Ag_2S_2O_7$ (~2.24 eV). However, compared with Ag_2O/TiO_2, the photocatalytic activity of $Ag_2O/Ag_2S_2O_7/TiO_2$ was slightly decreased due to the reduced content of Ag_2O. So, the relatively high and stable UV photocatalytic activity of $Ag_2O/Ag_2S_2O_7/TiO_2$ was obtained by the sulfur doping due to the protective effect and energy band structure of $Ag_2S_2O_7$.

Under visible light irradiation, Ag_2O, $Ag_2S_2O_7$ and Ag_2S can be excited to produce h^+ and e^- due to the narrow band gap (1.2 eV, 2.24 eV and 0.92 eV, respectively), leading to the apparent visible photocatalytic activity. Compared with Ag_2O/TiO_2 and $Ag_2S_2O_7/TiO_2$, the $Ag_2O/Ag_2S_2O_7/TiO_2$ heterostructure possessed the best visible photocatalytic activity. The results were mostly attributed to the heterostructure and energy band matching of Ag_2O and $Ag_2S_2O_7$. The lifetime of the excited electrons and holes was prolonged in the transfer process between heterostructures, thus the photocatalytic reaction was enhanced. As electron excitation did not occur in TiO_2 by visible light irradiation, Ag_2O and $Ag_2S_2O_7$ were stable in the system of $Ag_2O/Ag_2S_2O_7/TiO_2$. These characteristics led to the emergence of the $Ag_2O/Ag_2S_2O_7/TiO_2$ heterostructures as the best photocatalyst among the series.

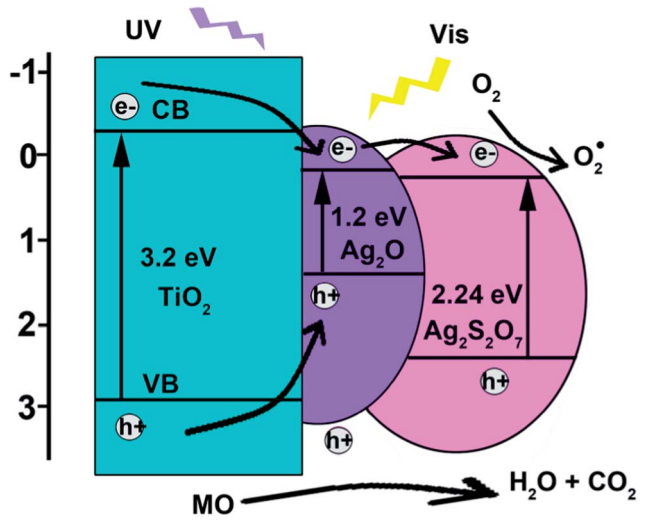

Fig. 9 A schematic view for the electron–hole separation and energy band matching of the $Ag_2O/Ag_2S_2O_7/TiO_2$ heterostructure under UV and visible light irradiation.

Conclusions

The $Ag_2O/Ag_2S_2O_7/TiO_2$ nanobelt heterostructures were synthesized by the S-doping of Ag_2O/TiO_2 nanobelts. The crystal structure and phase transformation of Ag_2O, $Ag_2S_2O_7$ and Ag_2S were studied by XRD and XPS measurements. XPS studies indicated that the sulfuration process involved various valence states of the S element, from S^{2-} (Na_2S) to S^{6+} ($Ag_2S_2O_7$), then to S^{2-} (Ag_2S). Within the present experimental context, the $Ag_2O/Ag_2S_2O_7/TiO_2$ heterostructured nanobelts exhibited high and stable photocatalytic activity under both ultraviolet and visible light irradiation. The UV-vis absorption spectra showed that Ag_2O, $Ag_2S_2O_7$ and Ag_2S served as effective visible-light sensitizers that led to the improved visible light photocatalytic activity of the TiO_2 nanobelts. The results might be accounted for by the energy band matching among Ag_2O, $Ag_2S_2O_7$ and TiO_2, as well as by the structure restriction effects.

Acknowledgements

This research was supported by the National Natural Science Foundation of China (50925205), the "100 Talents Program" of Chinese Academy of Sciences, the Recruitment Program of Global Experts, the PhD Start-up Funds of the Natural Science Foundation of Guangdong Province (S2013040016465), the Zhujiang New Stars of Science & Technology, and the Fundamental Research Funds for Central Universities, China.

Notes and references

1 A. Fujishima and K. Honda, *Nature*, 1972, **238**, 37–38.
2 L. K. Tan, M. K. Kumar, W. W. An and H. Gao, *ACS Appl. Mater. Interfaces*, 2010, **2**, 498–503.
3 H. Zhang, X. J. Lv, Y. M. Li, Y. Wang and J. H. Li, *ACS Nano*, 2010, **1**, 380–386.
4 W. J. Zhou, G. J. Du, P. G. Hu, G. H. Li, D. Z. Wang, H. Liu, J. Y. Wang, R. I. Boughton, D. Liu and H. D. Jiang, *J. Mater. Chem.*, 2011, **21**, 7937–7945.
5 W. J. Zhou, G. J. Du, P. G. Hu, Y. Q. Yin, J. H. Li, J. H. Yu, G. C. Wang, J. X. Wang, H. Liu, J. Y. Wang and H. Zhang, *J. Hazard. Mater.*, 2011, **197**, 19–25.
6 Z. G. Xiong and X. Song Zhao, *J. Am. Chem. Soc.*, 2012, **134**, 5754–5757.
7 R. Asahi, T. Morikawa, T. Ohwaki, K. Aoki and Y. Taga, *Science*, 2001, **293**, 269–271.
8 X. Chen, L. Liu, P. Y. Yu and S. S. Mao, *Science*, 2011, **331**, 746–750.
9 G. M. Wang, H. Y. Wang, Y. C. Ling, Y. C. Tang, X. Y. Yang, R. C. Fitzmorris, C. C. Wang, J. Z. Zhang and Y. Li, *Nano Lett.*, 2011, **11**, 3026–3033.
10 S. U. M. Khan, M. Al-Shahry and W. B. Ingler, *Science*, 2002, **297**, 2243–2245.
11 W. J. Zhou, H. Liu, J. Y. Wang, D. Liu, G. J. Du and J. J. Cui, *ACS Appl. Mater. Interfaces*, 2010, **2**, 2385–2392.
12 X. Q. Qiu, M. Miyauchi, K. Sunada, M. Minoshima, M. Liu, Y. Lu, D. Li, Y. Shimodaira, Y. Hosogi, Y. Kuroda and K. Hashimoto, *ACS Nano*, 2012, **2**, 1609–1618.
13 W. J. Zhou, Z. Y. Yin, Y. P. Du, X. Huang, Z. Y. Zeng, Z. X. Fan, H. Liu, J. Y. Wang and H. Zhang, *Small*, 2013, **9**, 140–147.
14 K. E. deKrafft, C. Wang and W. B. Lin, *Adv. Mater.*, 2012, **24**, 2014.
15 X. M. Zhang, K. F. Huo, L. S. Hu, Z. W. Wu and P. K. Chu, *J. Am. Ceram. Soc.*, 2010, **93**, 2771–2778.
16 B. Gao, J. J. Fu, K. F. Huo, W. R. Zhang, Y. H. Xie and P. K. Chu, *J. Am. Ceram. Soc.*, 2011, **94**, 2330–2338.
17 N. J. Borys, M. J. Walter, J. Huang, D. V. Talapin and J. M. Lupton, *Science*, 2010, **330**, 1371–1374.
18 X. F. Gao, W. T. Sun, G. Ai and L. M. Peng, *Appl. Phys. Lett.*, 2010, **96**, 153104.
19 H. F. Cheng, B. B. Huang, P. Wang, Z. Y. Wang, Z. Z. Lou, J. P. Wang, X. Y. Qin, X. Y. Zhang and Y. Dai, *Chem. Commun.*, 2011, **47**, 7054–7056.
20 X. F. Wang, S. F. Li, H. G. Yu, J. G. Yu and S. W. Liu, *Chem. – Eur. J.*, 2011, **17**, 7777–7780.
21 H. G. Yu, R. Liu, X. F. Wang, P. Wang and J. G. Yu, *Appl. Catal., B*, 2012, **111–112**, 326–333.
22 G. Wang, X. C. Ma, B. B. Huang, H. F. Cheng, Z. Y. Wang, J. Zhan, X. Y. Qin, X. Y. Zhang and Y. Dai, *J. Mater. Chem.*, 2012, **22**, 21189–21194.
23 M. Wu, J. M. Yan, M. Zhao and Q. Jiang, *ChemPlusChem*, 2012, **77**, 931–935.
24 L. Zhu, B. Wei, L. L. Xu, Z. Lü, H. L. Zhang, H. Gao and J. X. Che, *CrystEngComm*, 2012, **14**, 5705–5709.
25 D. Sarkar, C. K. Ghosh, S. Mukherjee and K. K. Chattopadhyay, *ACS Appl. Mater. Interfaces*, 2013, **5**, 331–337.
26 C. L. Yu, G. Li, S. Kumar, K. Yang and R. C. Jin, *Adv. Mater.*, 2014, **26**, 892–898.
27 Z. Y. Ji, X. P. Shen, J. L. Yang, Y. L. Xu, G. X. Zhu and K. M. Chen, *Eur. J. Inorg. Chem.*, 2013, **36**, 6119–6125.
28 M. Xu, L. Han and S. J. Dong, *ACS Appl. Mater. Interfaces*, 2013, **5**, 12533–12540.
29 P. Wang, B. B. Huang, X. Y. Qin, X. Y. Zhang, Y. Dai, J. Y. Wei and M. H. Whangbo, *Angew. Chem., Int. Ed.*, 2008, **47**, 7931–7933.
30 A. Paracchino, V. Laporte, K. Sivula, M. Grätzel and E. Thimsen, *Nat. Mater.*, 2011, **10**, 456–461.
31 X. G. Wen, S. H. Wang, Y. T. Xie, X. Y. Li and S. H. Yang, *J. Phys. Chem. B*, 2005, **109**, 10100–10106.
32 Z. H. Zhao, J. Tian, D. Z. Wang, X. L. Kang, Y. H. Sang, H. Liu, J. Y. Wang, S. W. Chen, R. I. Boughtond and H. D. Jiang, *J. Mater. Chem.*, 2012, **22**, 23395–23403.
33 Y. Xu and M. A. A. Schoonen, *Am. Mineral.*, 2000, **85**, 543–556.

